ARL-TR-10425 ● SEP 2026

The 1550-nm Tunable Photonic Integrated Circuit (PIC) External Cavity Laser (ECL)

by G. Alex Newburgh, Justin Bickford, Valerie Yoshioka, and Pak Cho

NOTICES

Disclaimers

ARL-TR-10425 ● SEP 2026

The 1550-nm Tunable Photonic Integrated Circuit (PIC) External Cavity Laser (ECL)

G. Alex Newburgh and Justin Bickford
DEVCOM Army Research Laboratory

Valerie Yoshioka
Oak Ridge Associated Universities

Pak Cho
General Technical Services

REPORT DOCUMENTATION PAGE

1. REPORT DATE	2. REPORT TYPE	3. DATES COVERED START DATE	3. DATES COVERED END DATE
September 2026	Technical Report	March 2024	July 2026

4. TITLE AND SUBTITLE
The 1550-nm Tunable Photonic Integrated Circuit (PIC) External Cavity Laser (ECL)

5a. CONTRACT NUMBER	5b. GRANT NUMBER	5c. PROGRAM ELEMENT NUMBER

5d. PROJECT NUMBER	5e. TASK NUMBER	5f. WORK UNIT NUMBER

6. AUTHOR(S)
G. Alex Newburgh, Justin Bickford, Valerie Yoshioka, and Pak Cho

7. PERFORMING ORGANIZATION NAME(S) AND ADDRESS(ES)	8. PERFORMING ORGANIZATION REPORT NUMBER
DEVCOM Army Research Laboratory ATTN: FCDD-RLA-PC Adelphi, MD 20783	ARL-TR-10425

9. SPONSORING/MONITORING AGENCY NAME(S) AND ADDRESS(ES)	10. SPONSOR/MONITOR'S ACRONYM(S)	11. SPONSOR/MONITOR'S REPORT NUMBER(S)

12. DISTRIBUTION/AVAILABILITY STATEMENT
DISTRIBUTION STATEMENT A. Approved for public release: distribution unlimited.

13. SUPPLEMENTARY NOTES

14. ABSTRACT
Widely tunable lasers operating at approximately 1550 nm are required for the implementation of compact atomic-based sensors, optical-based communication, and chemical/biological sensors. This report details the construction and characterization of a prototype 1550-nm tunable diode laser on a chip. The device occupies less than 1 mm^2 of area and is continuously wavelength-tunable in the range of 1530 to 1600 nm with a side-band suppression ratio of greater than 50 dB.

15. SUBJECT TERMS
Photonics, Electronics, and Quantum Sciences; hybrid integrated laser; 1550-nm tunable diode laser; external cavity diode laser; photonic integrated circuit

16. SECURITY CLASSIFICATION OF: a. REPORT	b. ABSTRACT	C. THIS PAGE	17. LIMITATION OF ABSTRACT	18. NUMBER OF PAGES
UNCLASSIFIED	UNCLASSIFIED	UNCLASSIFIED	UU	33

19a. NAME OF RESPONSIBLE PERSON	19b. PHONE NUMBER *(Include area code)*
G. Alex Newburgh	(520) 691-5698

STANDARD FORM 298 (REV. 5/2020)
Prescribed by ANSI Std. Z39.18

Contents

List of Figures

List of Tables

1. Introduction

The first compact tunable laser on a silicon (Si) chip was enabled by the integration of optically active gain medium with a photonic integrated circuit (PIC) (Chu et al. 2009). The PIC's external cavity functioned as an optical feedback control circuit to the gain medium; together, the ensemble forms an EC laser (ECL). As the gain medium is not grown at the same time of PIC fabrication, the laser is classified as a heterogeneous ECL (Roelkens et al. 2024).

ECLs have been used in a wide range of applications, including telecommunications, light detection and ranging, free space optical links (Coldren et al. 2022), chemical/biological sensing (Strandberg et al. 2025), precision clocks (Newman et al. 2019), and quantum sensing and information processing (Elshaari et al. 2020). These applications often require wide wavelength tunability of the laser from the visible to near-IR, along with high wavelength precision. They are an attractive alternative with smaller cost and size compared with benchtop tunable laser sources. The promise of greater miniaturization of PIC-based ECLs can be expected, as the PIC component density increase follows Moore's law (Smit et al. 2019).

This report details the design and characterization of the U.S. Army Combat Capabilities Development Command (DEVCOM) Army Research Laboratory's (ARL's) first 1550-nm compact, tunable, narrow-line-width ECL. We have used our cooperative agreements with our partners at Dream Photonics in Vancouver, Canada, and the Air Force Research Laboratory at Wright–Patterson Air Force Base, Ohio, to connect PICs to gain material by "writing" a photonic wire bond (PWB) as well as achieving the modeling and discussion of experimental results.

2. The 1550-nm Reflective Semiconductor Optical Amplifier (RSOA) ECL

A photomicrograph of the optical gain medium (1550-nm RSOA) PWBed to a PIC is shown in Figure 1. The 250-µm-long PWB serves to guide the light leaving the 1550-nm RSOA gain medium (on the left) to the external cavity (on the right). The External cavity portion of the ECL is represented by an image of the layout file for manufacture by the American Institute for Manufacturing Integrated Photonics (AIM). A detailed image of the layout file is shown in Figure 2. The external cavity circuit comprises a longitudinal mode tuner (LMT), directional coupler (DC), and tunable Vernier ring (VR) pair of 8- and 9-µm-diameter ring resonators (RRs). The LMT, DC, and VRs' optical characteristics can be thermally tuned. Resistive heaters adjacent to the LMT, Mach–Zehnder interferometer (MZI), DC, and VRs' wave guide components allow for dynamic tuning of those elements through the thermo-optic properties of the wave guide media.

The LMT is used to fine-tune the optical path length (OPL) of the external cavity and thereby fine-tune the resonant laser wavelength of the external cavity. The VR acts as a tunable optical filter and is used to select a unique lasing wavelength within the entire optical gain spectrum of the RSOA. The DC component allows the user to select the optimum level of optical feedback to the RSOA and thereby optimize laser performance.

The fraction of light that leaves the laser cavity by way of the topmost arm of the DC is divided into two portions by the 98/2 splitter. Ninety-eight percent of the laser light is directed off-chip while 2% is intercepted by a Ge PD, used to monitor on-chip laser intensity.

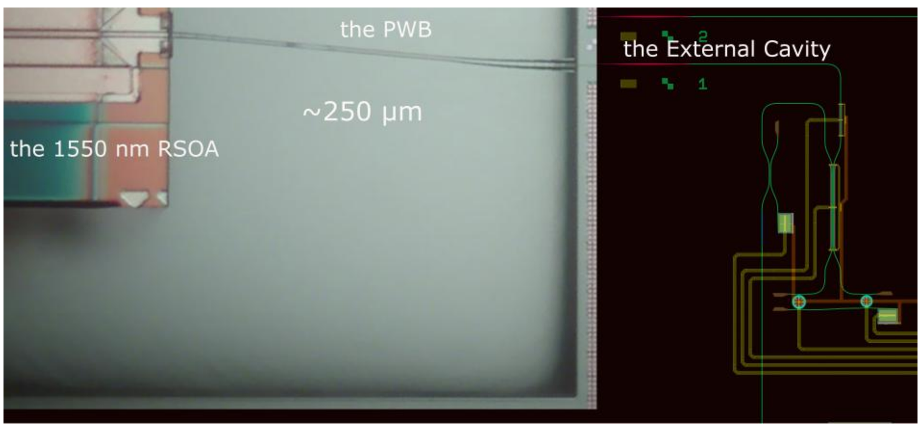

Figure 1. 1550-nm RSOA ECL with PWB.

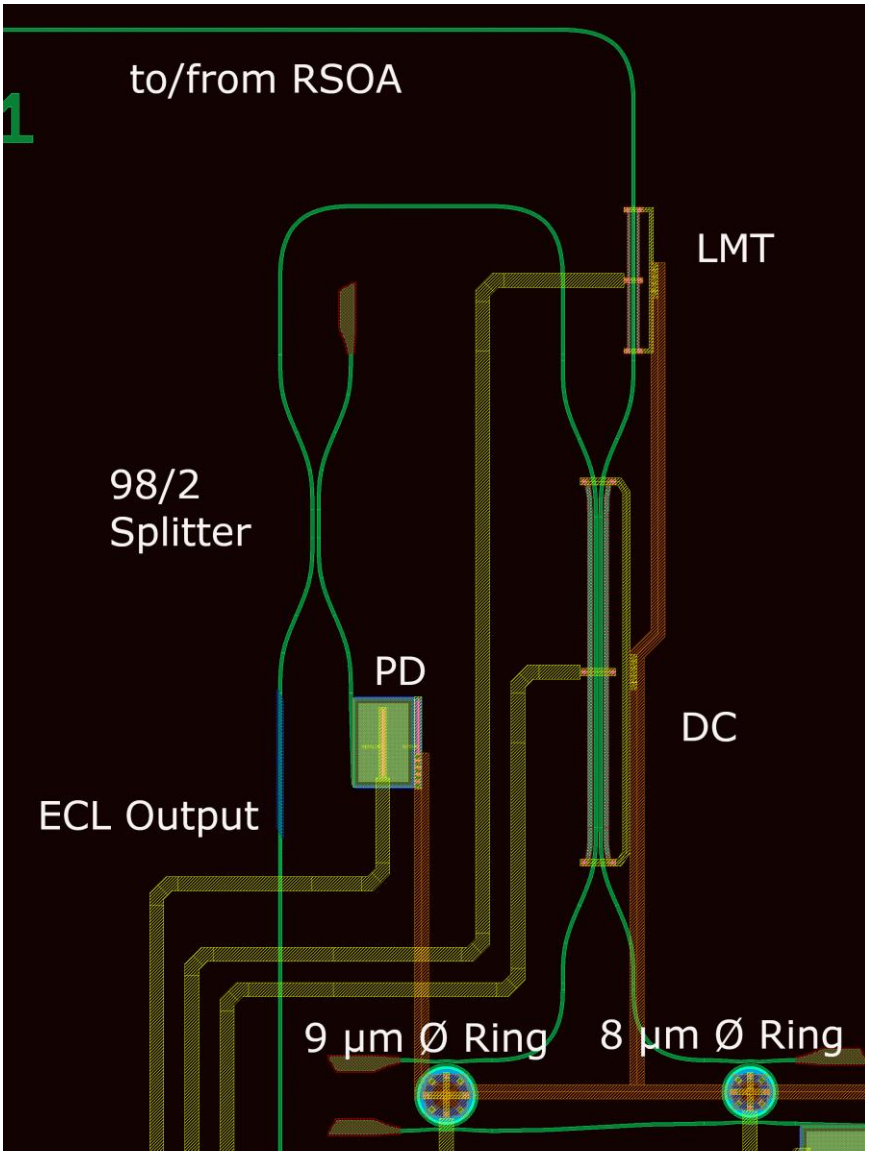

Figure 2. Detail of 1550-nm RSOA ECL showing the PIC components used (LMT, DC, and VR pair). The 98/2 splitter directs ~98% of the light off-chip, while 2% is captured by the Germanium (Ge) photodiode (PD) as a monitor of lasing intensity. Brown trace = electrical ground, green trace = Si optical wave guide, yellow trace = electrical signal.

2.1 The 1550-nm RSOA

An indium–gallium–arsenide–phosphide multiple quantum well RSOA was selected as the laser gain element for the ECL. The chip measured 250 µm in width by 1 mm in length. A pick-and-place instrument was used by ARL to locate the RSOA in the PIC pocket, as shown in Figure 1. Location of the chip was to within 2 µm spatially and 1° in angular orientation, as measured after placement using the microscope image. The gain chip was attached to the PIC with an electrically conductive silver epoxy. The manufacturer of the RSOA characterized the gain medium to have an amplified spontaneous emission (ASE) bandwidth of 50–70 nm and an ASE optical power of 1.2 mW at 300 mA injection current (the maximum rated current is 350 mA). The back facet reflection coating was rated to be greater than 90% and the effective reflectivity of the front facet to be less than 0.1%. Under laser operation, the RSOA optical power can be as high as 40 mW.

2.2 The 1550-nm PWB and Edge Coupler (EC)

The PWB is a 3D-nanoprinted optical wave guide and was used to optically couple the semiconductor gain element to the external cavity. The PWB transfers the light of the gain medium to and from the PIC external cavity wave guide. The PWB must be long enough to convert the spatially wide, low-numerical aperture (NA) RSOA emission profile to the relatively spatially narrow, high-NA external cavity EC wave guide adiabatically. As guide for designing an adiabatic taper, the Milton rule of thumb specifies that the NA of the mode is less than $\lambda /(2W)$, where W is the widest point of the wave guide and λ is the wavelength of light (Milton and Burns 1977).

ARL's 1550-nm EC is designed to accept 1550-nm single-mode transverse electric polarized light in a 5-µm mode field diameter (MFD) and adiabatically convert the mode to a 400-nm wide, 220-nm high Si wave guide. The EC consists of two tapered Si nitride (SiN) (n = 2) wave guides stacked on an Si (n = 3.3) wave guide (Figure 3) embedded in an Si dioxide (SiO_2) (n = 1.45) cladding. At the face of the EC, a 5-µm injected mode experiences a wave guide consisting mostly of oxide with a subwavelength portion of SiN at center. The SiN portion of the wave guide can be thought of as a crude form of gradient doping of the SiO_2, similar to a continuously gradient doped fiber.

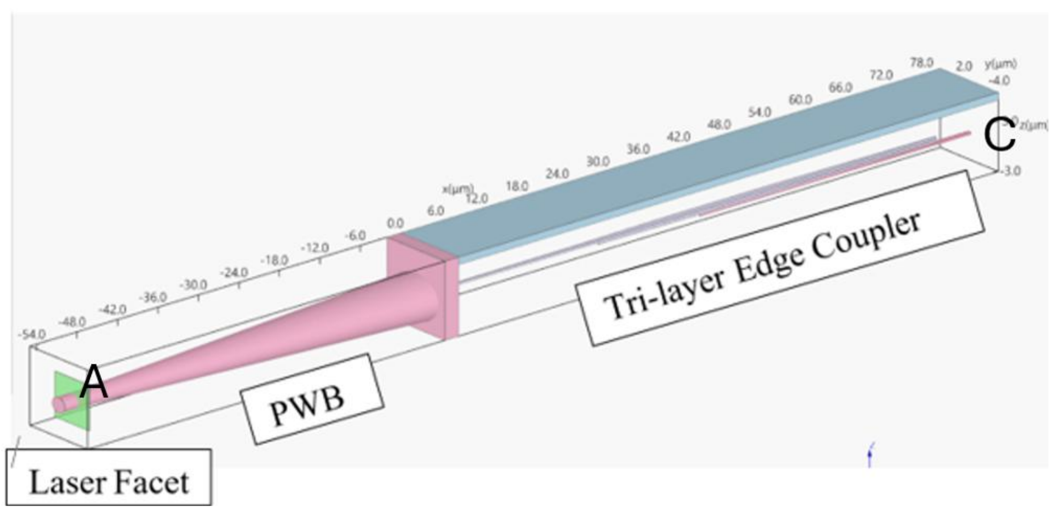

Figure 3. Simulation model of PWB design. The PWB-to-wave guide transmission loss is 2.25 dB. The PWB core is 7.8 × 5.6 µm.

As the injected light travels along the EC axis, the high refractive index SiN core begins by "capturing" the injected light and, through gentle adiabatic tapering, confines most of the light to itself. As the eventual goal is to bring the light to the Si wave guide, the second underlying SiN is used to "ladder down" the captured light to the Si wave guide, which lies just under the second SiN wave guide. The EC was designed to accept 5-µm MFD to the PIC Si wave guide with approximately a 2.25-dB penalty. An example of the PWB/Si + first nitride + second nitride trilayer design is shown in Figure 3, which details the process of accepting light from the laser facet (A) to its transfer to Si wave guide (C).

3. The Longitudinal Mode Tuner

The PIC, as shown in Figure 2, includes an LMT. The LMT enables the tuning of the OPL of the external cavity by altering the refractive index of the LMT wave guide. Heating of the Si wave guide is made by fabricating a resistive heater 150 nm adjacent to the wave guide. As the thermo-optic coefficient of Si, $dn/dT = 1.85 \times 10^{-4}\ [K^{-1}]$ (Xu et al. 2019), is positive, the heating of the LMT can only increase the effective length of the external cavity. As a means of estimating how much LMT heating, $\Delta T\ [K]$, is required to tune an optical phase shift of $\Delta\phi = \pi$, we can use the relation

$$\frac{\lambda}{2} = L\frac{dn}{dT}\Delta T \tag{1}$$

where the length of the LMT heater, $L = 20\ \mu m$, requires heating by approximately $\Delta T = 207\ K$.

The 3-tap LMT wave guide heater was characterized, and it was found that a phase shift of $\Delta\phi = \pi\ \&\ 2\pi$ (Figure 4) was achieved for applied voltages of $V_{\pi} = 5.7\ V$ $(P = 17\ mW)$ and $V_{2\pi} = 8.9\ V$, respectively. It was observed that the shift remained linear when heating up to a maximum voltage, $Vmax = 10.5\ V$, and that a breakdown voltage of $V = 11\ V$ resulted in damage to the device. A maximum phase shift $\Delta\phi = 2.6\ \pi$ was achieved using applied electrical power equal to $P = 44.1\ mW$.

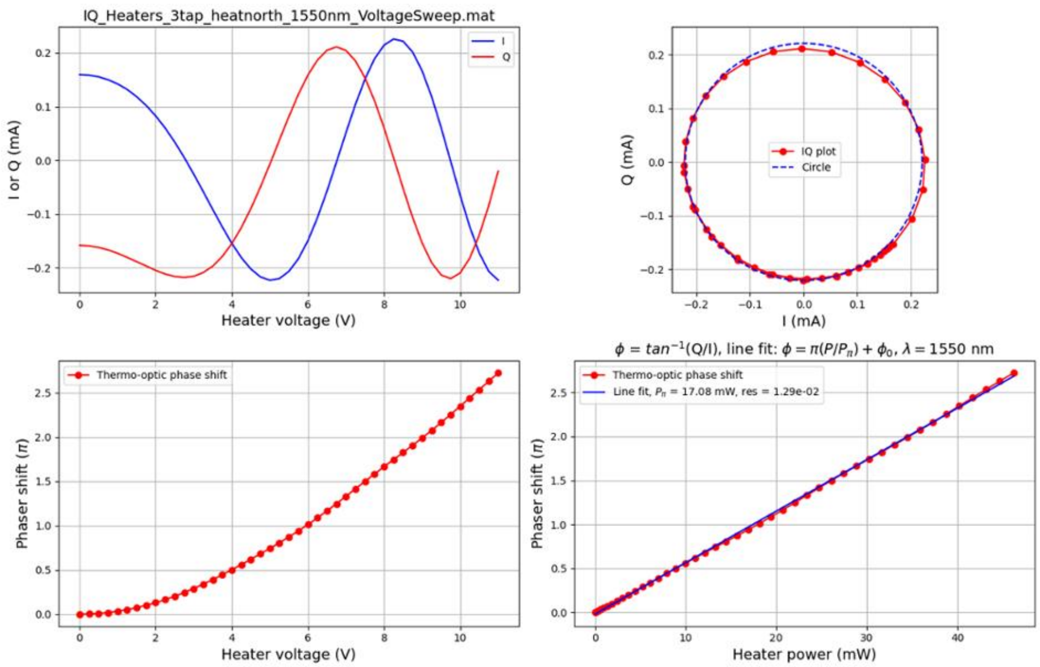

Figure 4. LMT phase tuning as a function of heater power.

4. Thermally Adjustable DC

The 50-µm-long DC was used by the external cavity to adjust the fraction of light returned to the RSOA. By heating the body of the DC, the splitting ratio of the DC outputs can be regulated. We began by characterizing the wavelength dependence of the unheated DC. The fraction of light remaining in the wave guide ("bar") (Figure 5) and that crossing over ("cross") to the parallel wave guide of the DC was measured and fit using a sinusoid (Figure 6a). The DC was shown to have a dynamic range close to (0%–100%) with a period of 415 nm. We measured the splitting response of the DC to heating at 1550 nm (Figure 6b), demonstrating that the splitting ratio was periodic with a heating voltage of 33.4 V.

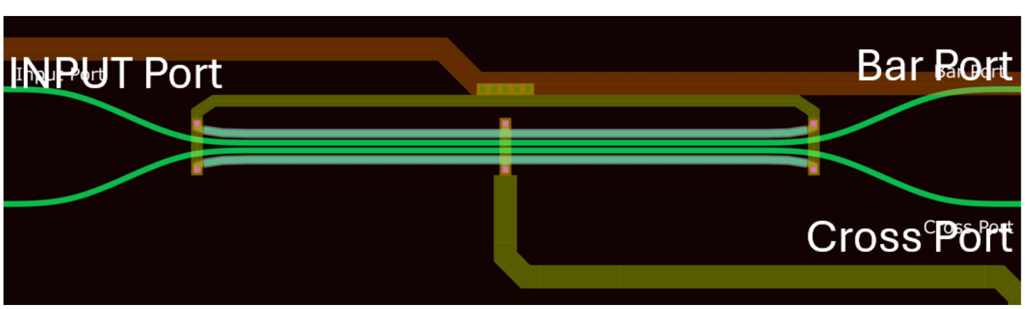

Figure 5. Detail of the DC showing bar and cross ports.

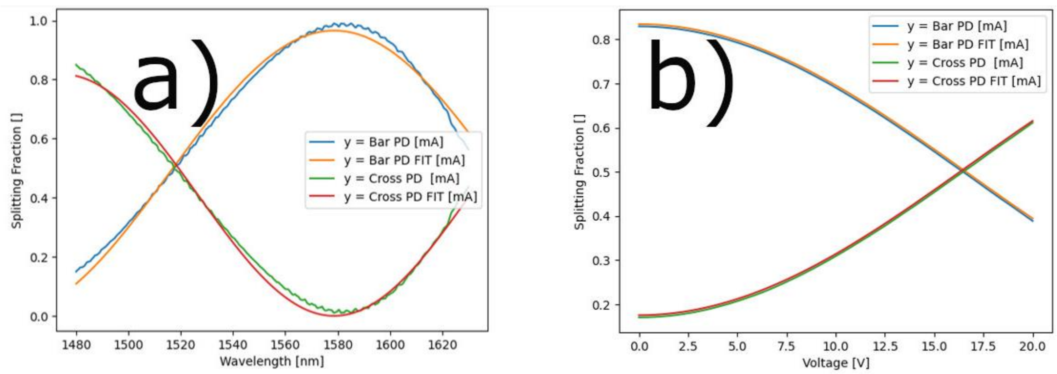

Figure 6. a) Plot of the DC fraction in cross and bar wave guides as a function of wavelength. The period of the sinusoid is 415 nm. b) Response of the DC to heater voltage at 1550 nm. Fit with sinusoid demonstrating minimum cross-splitting values of 17%. The bar response fit as 0.674 × $\sin^2$(0.047 × (V – 33.413)) + 0.155. The cross response fit as 0.674 × $\sin^2$(0.047 × (V +0.18)) + 0.17. A $V_{2\pi}$ = 33.4 V is derived from the 0.047 coefficient.

5. The VR Component

The VR component is constructed of two optically connected, high-Q RRs of different radii. The VR behaves as a narrow optical bandwidth pass filter. By adjusting the 8- and 9-µm rings' heaters to optically resonate at the same wavelength, the VR passes only a single wavelength, thereby ensuring a single lasing wavelength.

Taken by itself, an individual ring of radius, *R,* transmits a set of wavelengths of near equal wavelength spacings, called the free-spectral range (FSR); $FSR = \lambda^2/(n_g 2\pi R)$. By optically linking the two RRs of different radii, R_1 and R_2, a new (compound) spectral filter is made such that the two rings line up at a larger interval of $(FSR\_VR) = \lambda^2/ n_g 2\pi (R_2 - R_1)$. In the case at hand for $n_g = 3.8$, $FSR\_VR \approx 200$ nm.

5.1 The 8-µm-Diameter Ring

The 8-µm-diameter ring (see Figure 2) is designed to couple to a wave guide placed at 180 nm away through a "pulley" configuration. The proximity (subwavelength distance) of ring to the bus straight wave guide allows for a small portion of the light to be transferred from pulley wave guide to the ring wave guide. The degree to which a particular wavelength exits the ring, either from the top (thru port) or the bottom (drop port), depends on whether an integer number of wavelengths fits along the ring circumference (i.e., in resonance with it). Assuming no loss in the ring, the sum of the drop- and through-port powers equal the power incident on the ring. In practice, the sum of the through-port and drop-port light powers is approximately 95%.

The wavelength filtering response of the 8-µm-diameter ring is presented in Figure 7a and shows an FSR of approximately 26.2 nm. Given the diameter of the ring, a group index of 3.8 is estimated. Figure 7b summarizes ring FSR as a function of wavelength with a linear fit.

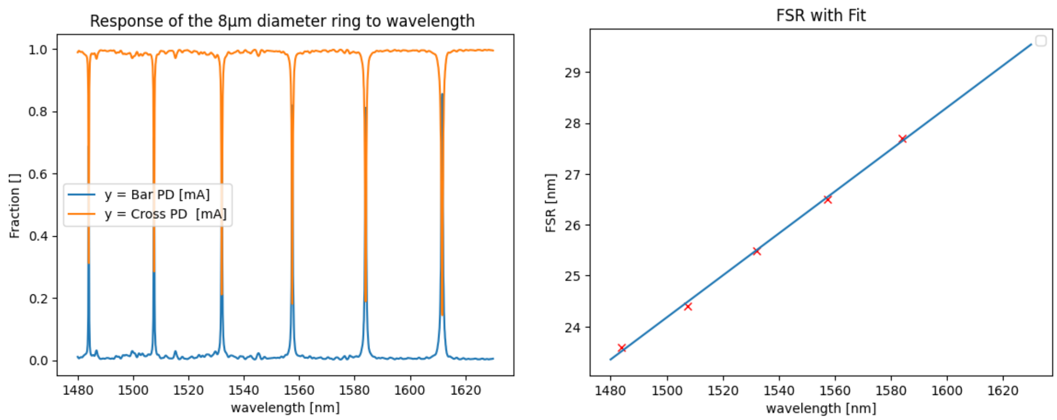

(a) (b)

Figure 7. a) Response of 8-µm ring to a wide wavelength sweep. b) Ring FSR as a function of wavelength with fit, FSR (λ) = 26.2 + 0.0412 × (λ-1549.1) (nm).

The RRs' resonant wavelength can be tuned by applying a voltage to the concentric heaters, as shown in Figure 8. The peak displacement is linear with heater power, P, and can be fit as $\lambda_{peak}(P) = 1557.186 + 0.7713\ P\ (mW)$.

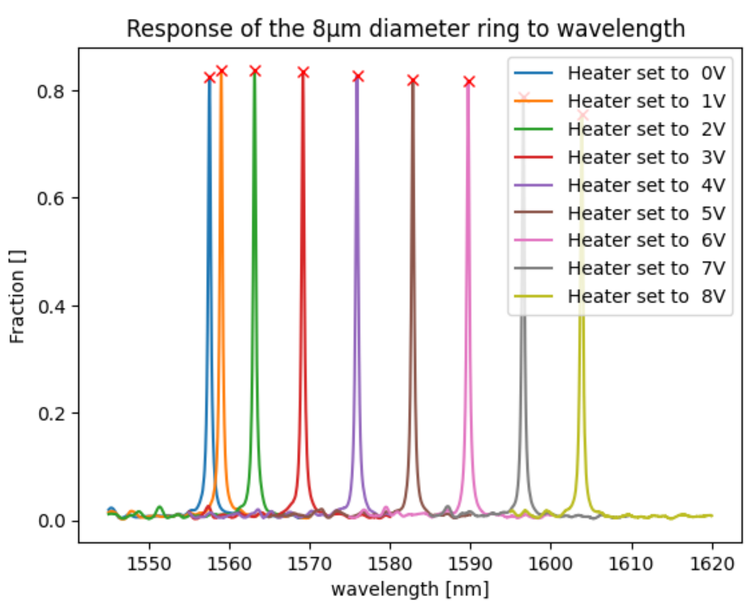

Figure 8. Tuning response of the 8-µm ring tuning with heater voltage.

Using the relation that

$$FSR(\lambda_0) + \left(\frac{d\, FSR(\lambda)}{d\lambda}\middle|\lambda = \lambda_0\right)(\lambda - \lambda_0) =$$

$$\frac{\lambda_0^2}{2\,\pi R n_{eff}} - \frac{(\lambda - \lambda_0)\left(\frac{dn}{d\lambda}\lambda_0^2 - 2\, n_{eff}\lambda_0\right)}{2\,\pi R n_{eff}^2} \tag{2}$$

and identifying the constants of the fit (Figure 7b) allows us to describe the group index 8-µm-diameter ring as

$$n_g(\lambda, P) = n_{eff}\left(1 + \frac{\frac{d\lambda}{dP}}{\lambda} P\right) + \frac{dn}{d\lambda}(\lambda - \lambda_0) + \frac{dn^2}{d\lambda^2}(\lambda - \lambda_0)^2$$

$$= 3.8174\left(1 + \frac{0.7713}{\lambda} P\right) + 1.0868 * 10^{-3}(\lambda - 1555.75)$$

$$+3.5 * 10^{-6}(\lambda - 1555.75)^2 \tag{3}$$

It is also possible to extract the coupling ring strength from the line width of the ring resonance (Figure 9). Using the idealized calculated response of the 4-port RR under the assumption that the drop-port wave guide is identical to the input wave guide, the drop and through intensities can be written as

$$Drop(\lambda, n_g, A, t) = (A\,(1-t)^2(1+t)^2)/(1 - 2\,t^2\cos\left(\frac{4\,\pi^2\,R\,n_g}{\lambda}\right) + t^4)) \tag{4}$$

$$Thru(\lambda, n_g, A, t) = \left(A\,t\frac{(1+t^2)\left(1 - \cos\left(\frac{4\pi^2\,R\,n_g}{\lambda}\right)\right)}{1 - 2\,t^2\cos\left(\frac{4\pi^2\,R\,n_g}{\lambda}\right) + t^4}\right) \tag{5}$$

where *t* is the through-port transfer coefficient and *A* is the input light amplitude. Using Equation 4 and fitting the plot in Figure 9, we find that *t = 0. 97416*, meaning that the ring bus wave guide couples $(1 - t^2) = 0.05$ (5%) of the bus power. The value of *t* can then be used to calculate the full width at half maximum (FWHM) line width of the ring resonance, $\Delta\lambda_{FWHM} = 435\ pm$, from the equation below:

$$\lambda_{FWHM} = 2\frac{\left(\pi - \cos^{-1}\left(\frac{t^4 - 4\,t^2 + 1}{2\,t^2}\right)\right)\lambda^2}{4\,\pi^2\,n\,R} \tag{6}$$

as well as the ring quality factor, *Q = 3585,* from the expression below:

$$Q = \frac{\lambda}{\lambda_{FWHM}} \tag{7}$$

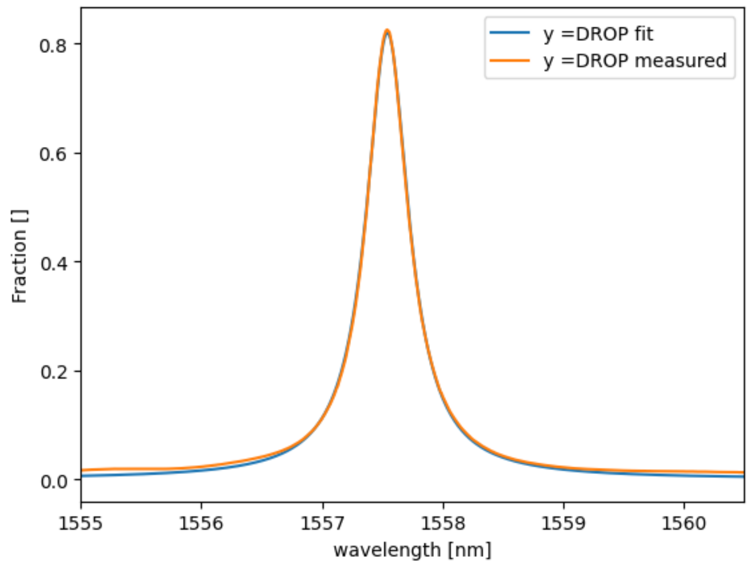

Figure 9. Drop-port response to wavelength swept input showing a FWHM line width of 435 pm.

5.2 9-µm-Diameter Ring Characterization

The second ring with 9-µm-diameter was measured for its response to a wavelength sweep from 1480–1630 nm. As expected, the FSR of the ring was smaller than the 8-µm-diameter ring, as the FSR is inversely proportional to the ratio of their diameters.

Fitting of the resonance at 1553 nm results in a line width FWHM = 551 nm, Q = 2820, and t = 0.9629 (a power coupling fraction of 7.2%). After running a fit of FSR (Figure 10, left), we find n_{eff}= 3.815, dn/dλ = –1.00075 × 10^{-3}, $dn^2/d\lambda^2$ = 3.15 × 10^{-6} where λ_0 = 1567.2.

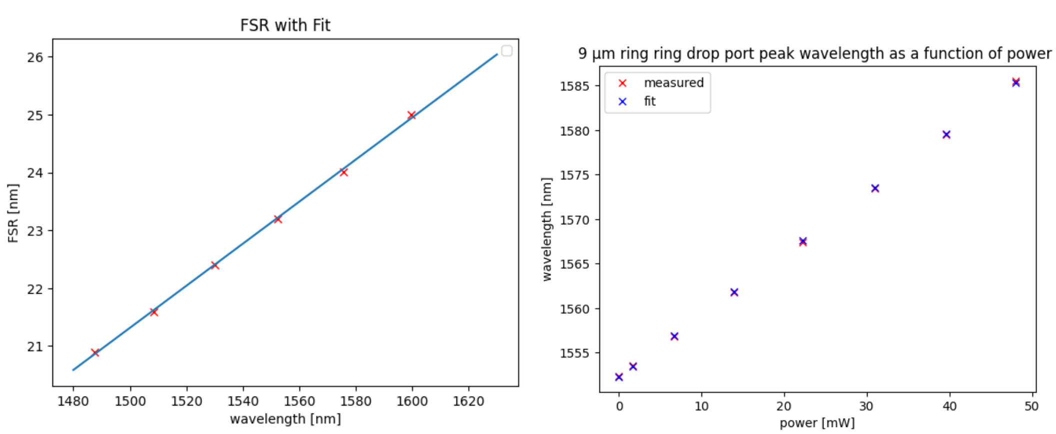

Figure 10. Left, plot FSR of the 9-µm-diameter ring. Fit of FSR (λ) = 19.63 + 0.03635 × (1454 – λ). Right, fitting of the peak positions as a function heater power. Δλ (P) = 1552.2667 + dλ/dP × P (mW), where dλ/dP = 0.6889.

(U) The results of thermally tuning of the 9-µm ring is plotted as a function of heater voltage. We can now describe the group index of the 9-µm ring as a function of power, P, as

$$n_g(\lambda, P) = n_{eff}\left(1 + \frac{\frac{d\lambda}{dP}}{\lambda} P\right) + \frac{dn}{d\lambda}(\lambda - \lambda_0) + \frac{dn^2}{d\lambda^2}(\lambda - \lambda_0)^2 \tag{8}$$

$$= 3.815\left(1 + \frac{0.6889}{\lambda} P\right) + 1.0075 \ * \ 10^{-3}(\lambda - 1567.2)$$
$$+ 315 \ * \ 10^{-6}(\lambda - 1567.2)^2$$

where λ is nm and P is mW, The optical characteristics and the tuning of the 8- and 9-µm diameter rings as a function of ring heater powers are summarized in Table 1.

Table 1. Optical characteristics derived from the VRs.

Formula Description	**8-µm ring**	**9-µm ring**
Ring design name	rr_switch_pulley_thru_pulley_drop_4port	rr_switch_pulley_thru_pulley_drop_4port_9umD
FSR fit (nm)	$26.2 + 0.412 \times (\lambda - 1549.1)$	$19.63 + 0.03635 \times (\lambda - 1454)$
Group index derived from FSR fit	$n_g(\lambda) = 3.8174 - 1.0868 \times 10^{-3} \times (\lambda - 1555.85) + 3.5 \times 10^{-6} \times (\lambda - 1555.85)^2$	$n_g(\lambda) = 3.815 - 1.0075 \times 10^{-3} \times (\lambda - 1567.2) + 3.15 \times 10^{-6} \times (\lambda - 1567.2)^2$
FWHM/*Q*	435/3585	551/2820
Ring *t* transmission coefficient/ring power coupling fraction	0.97416/5.1%	0.9629/7.2%
Ring wavelength tuning as a function of heater power, *P* (nm)	$\Delta\lambda(P) = 1557.186 + 0.7713 \times P$ (mW)	$\Delta\lambda(P) = 1552.257 + 0.6889 \times P$ (mW)
Group index as a function of heater power, *P*, and wavelength, λ	$3.8174 \times (1 + 0.7713/\lambda \times P) + (-1.0868 \times 10^{-3})(\lambda - 1555.75) + 3.5 \times 10^{-6} (\lambda - 1555.75)^2$	$3.815 \times (1 + 0.6889/\lambda \times P) + (-1.0075 \times 10^{-3}) (\lambda - 1567.2) + 3.15 \times 10^{-6} (\lambda - 1567.2)^2$

5.3 9-µm-Diameter Ring Map

The spectral response of the heated 9-µm-diameter ring as measured at the thru port, is presented in Figure 11. A Santec TSL570 tunable semiconductor laser was used as an input to the external cavity circuit. We recorded the wavelength peaks by sweeping input wavelength and monitoring an onboard PIC PD. This process was repeated over a range of 9-µm-diameter ring heater voltage settings (0–7 V).

Examination of the plot shows a series of curves in parallel. In wavelength, they are spaced approximately 23 nm apart at 1550 nm, which is the expected FSR for the 9-µm-diameter ring. Reading vertically in voltage, we see that heating the ring from 0 to 5 V tunes the ring by a full FSR.

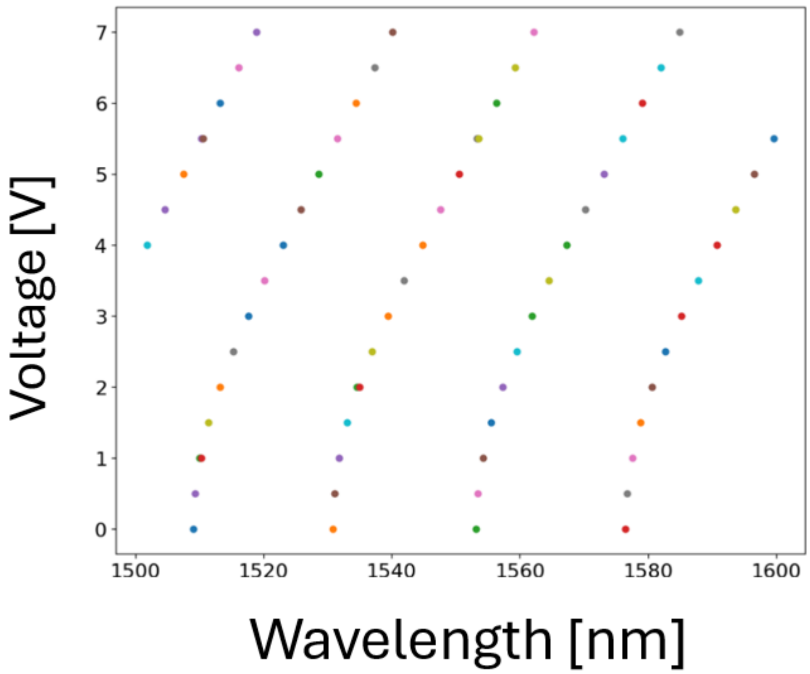

Figure 11. Map of the transmission for the 9-µm-diameter ring as a function of wavelength (x-axis) and heater voltage (y-axis).

We had observed that the (thermal) tuning of an individual Vernier component ring would change the resonant wavelength of the other ring. This is due to "thermal cross talk" between rings due to the migration of heat from one ring to the other through the PIC substrate. While a small effect, the shifting of hundreds of picometers is possible due to the thermal cross talk. The wavelength shift in the 9-µm ring due to the heating of the 8-µm ring as a function of heater power is shown on the left of Figure 12 and vice versa on the right. The wavelength tuning of 8-µm ring as a function of heating the 8-µm ring is shown on the left of Figure 13, while the right side shows the response of the 9-µm ring to heater power. From the fits of Figures 12 and 13, we conclude that thermal cross talk is on the order of 1%–2% in the ring tuning influence.

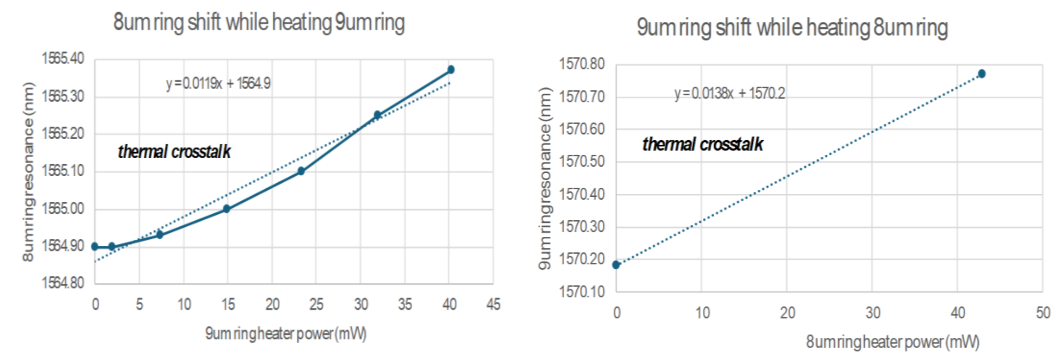

Figure 12. Left, the influence of the heating of 9-µm ring on the resonant wavelength of the 8-µm ring (thermal cross talk), and the converse on the right.

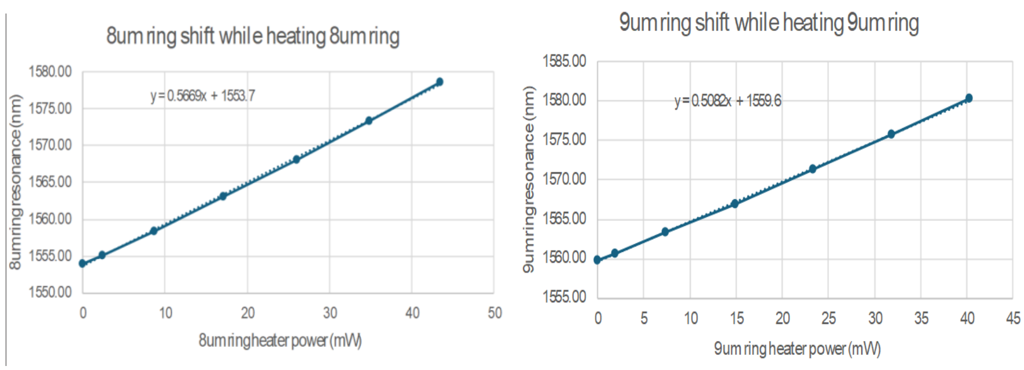

Figure 13. The wavelength tuning response of 8-µm ring (left) and the 9-µm ring (right) due to applied heater power.

6. Performance of the 1550-nm RSOA ECL

Initial experiments focused on determining the laser wavelength tuning range of the 1550-nm RSOA ECL. The ECL performance was sampled in 10-nm wavelength increments from 1530 to 1610 nm. The relative power was measured by coupling light off-chip to the Yokogawa AQ6370C Optical Spectrum Analyzer (OSA) (Figure 14, left). The FWHM of the laser gain profile was 50 nm and centered at 1585 nm.

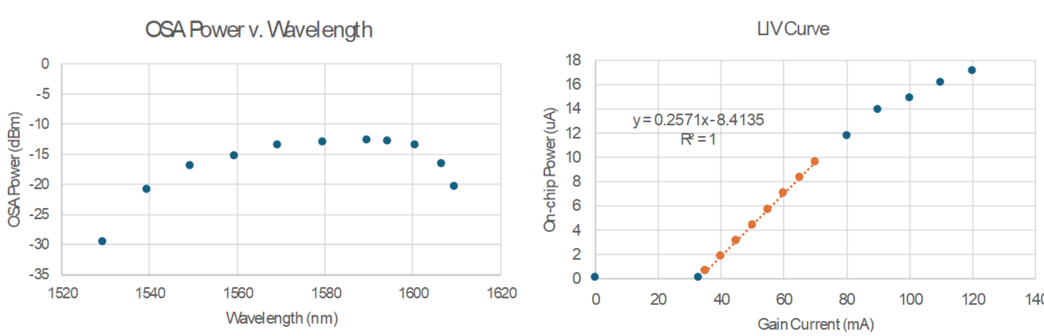

Figure 14. Left, ECL RSOA performance between the wavelength range of 1530 to 1610 nm. Right, LIV performance as tuned to lase at 1550 nm.

The ECL output power was sampled by the 2% trunk of the 98/2 splitter using the onboard PD. Figure 14, right, shows that the laser had a threshold of approximately 32.7 mA at 1550 nm. Additional current caused optical power to rise linearly until approximately 70 mA (1.3 V) of injection current. Accounting for the fact that the splitter routes approximately 2% of the light exiting the ECL to the PD and assuming a PD has a 1 A/W response, the laser efficiency is approximately 1.25%. The best laser performance occurred at 1585 nm with an electrical-to-optical (EO) efficiency of approximately 6%.

The laser spectral profile was measured by the OSA and is shown in Figure 15. A side mode suppression ratio (SMSR) equal to 60 dB was demonstrated with a line width limited by the stated resolution of the OSA of 20 pm. The two side bands approximately 75 pm from peak emission are attributed to the ECL cavity modes. The more prominent side bands (Δλ ≈ 375 pm) are most likely due to the gain cavity mode.

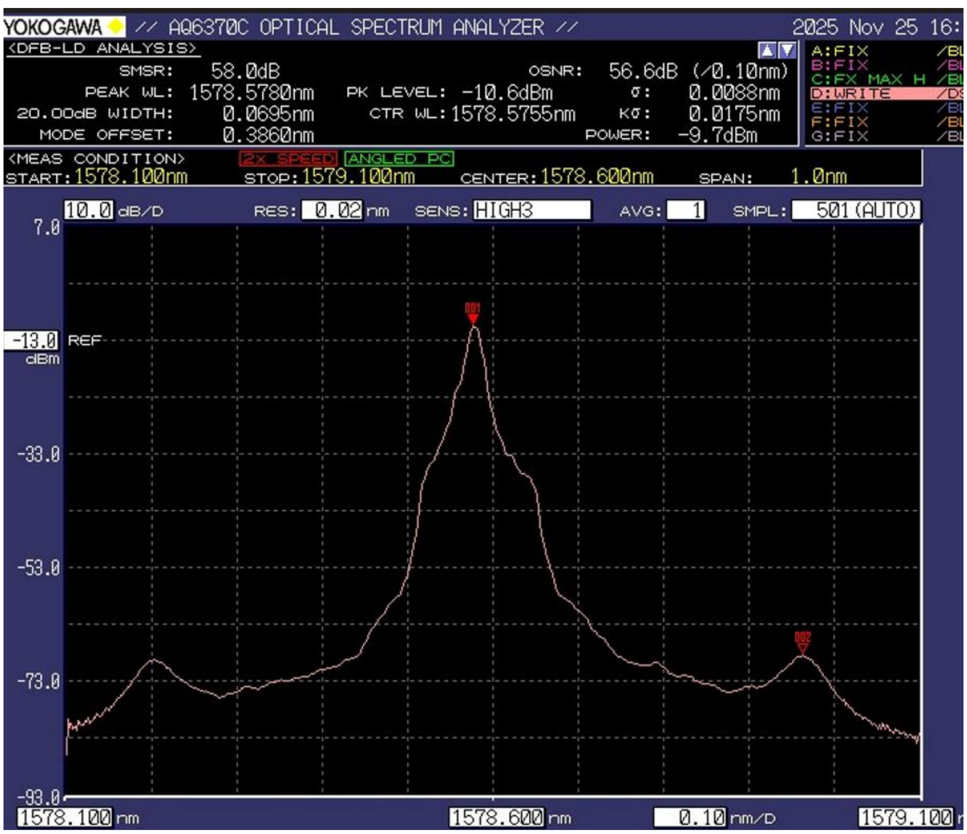

Figure 15. Spectral output of the RSOA ECL demonstrates excellent SMSR of 60-dB side bands (Δλ ≈ 375 pm). Side bands are attributed to the cavity modes of the gain medium.

7. The Second 1550-nm RSOA ECL Design

A second version of the 1550-nm RSOA ECL was assembled and tested from the June 2025 AIM run designated by the foundry as "Luke." Three important changes to the first 1550-nm ECL design were made:

1) The DC was exchanged for an MZI, allowing for less throughput loss and a more uniform response over the lasing wavelength range.
2) The pulley ring heater design of the March 2024 run was changed in the June 2025 run for straight-wave guide coupling. The June 2025 heaters were also designed with a slightly smaller radius so that heater-to-ring separation was increased to 175 nm. The separation of heater ring to wave guide reduced the optical coupling of heater to wave guide at the expense of heating efficiency.
3) The splitter was changed to a 90/10 design so that 90% of the light leaving the laser would be directed to an on-board PD and 10% is directed off-chip for greater sensitivity in off-chip measurements.

The layout of the second 1550-nm RSOA ECL design is shown in Figure 16. The multi-mode interferometer (MMI) functions as a broadband optical splitter required for both ends of the MZI. The higher-order mode (HOM) block component functions as an optical filter for light propagating along the waveguide.

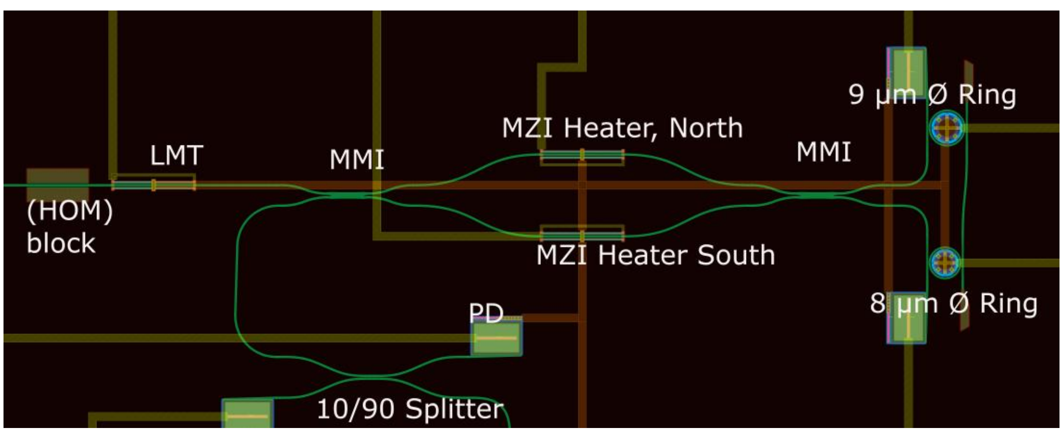

Figure 16. Schematic of the second 1550-nm RSOA ECL using an MZI instead of a DC for ECL reflectivity tuning.

8. The MZI Component

The transmission of the MZI was measured by tuning the VR pair to be resonant at 1550 nm. The voltage on the north heater was then swept from 0 to 5 V (0–22.5 mW). The received signal was monitored by the 8-µm ring thru port PD.

Alternatively, the south heater was swept, and the laser intracavity power monitored by the same PD, as shown in Figure 17. The response shows heater $P_{2\pi} \approx 39\ mW$ and that the MZI arms were slightly unbalanced at rest without heating. The MZI could be balanced through the addition of 6 mW of power to the south heater.

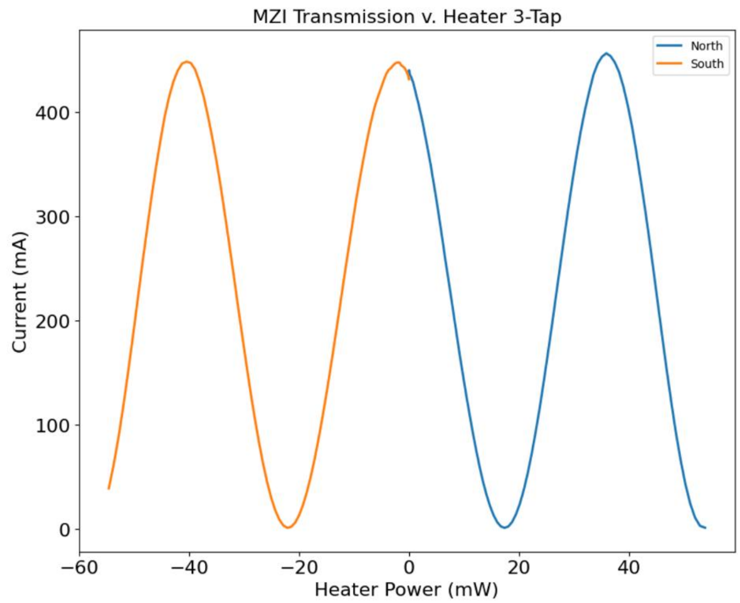

Figure 17. Signal received by 8-µm ring as north and south heaters are tuned independently using 1550-nm light injected into the ECL.

A second experiment was conducted whereby the RSOA was powered and the MZI heaters were sequentially swept and the intracavity laser power was monitored by the on-chip PD (Figure 18). The laser performance could be fit by $f(P) = sin(P - P_{offset})^2$, where P is the heater power and $P_{offset} = 4\ mW$ is the power required to balance the MZI.

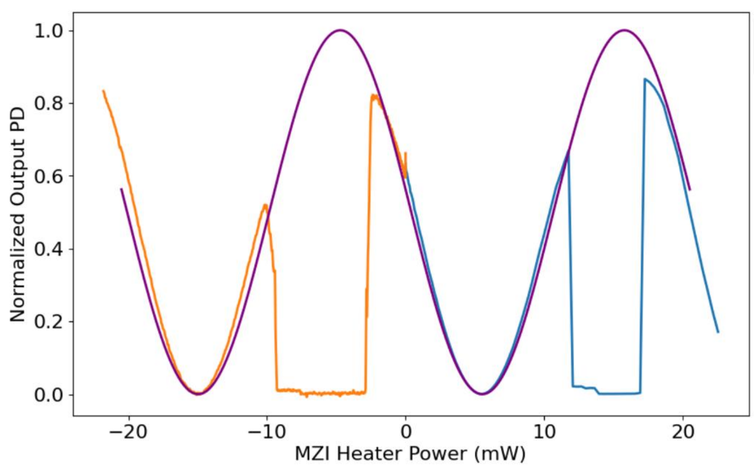

Figure 18. ECL intracavity power as MZI heaters independently tuned (north heater = blue, south heater = orange). Purple indicates an overlay of $R(P) \approx sin^2(P - 6)$.

Using the sinusoidal fit (purple trace) of the laser power, minimal laser intensity exits the cavity when maximal when cavity reflectivity occurs at $P_{North}= 5\ mW$ and $P_{South} = 15\ mW$. The south heater power values are defined as negative for purpose of plotting in Figure 18. At $P_{North}= 15\ mW$ and $P_{South} = 5\ mW,$ a region of the laser power is zero due to subthreshold lasing (reflectivity is zero). We can quantify the external cavity reflectivity, *R_reflect*, as

$$R\_reflect = \frac{1 - \cos(2(\varphi_{North} - \varphi_{South}))}{2} = sin^2(\varphi_{North} - \varphi_{South}) \quad (9)$$

where φ_{South} and φ_{North} are the phase delays due to heating of the south and north MZI heaters, respectively. From Figure 18, optimal lasing power occurs when the MZI is unbalanced by approximately 50°. Using Equation 9, this corresponds to a reflectivity of approximately 60%.

The response of the RSOA to the external cavity reflectivity (i.e., MZI heater voltage) of Figure 18 had not been optimized for laser cavity length. However, the laser cavity length can be adjusted by tuning the LMT to compensate for the optical length difference induced by heating of the MZI. The response of the ECL to MZI tuning and the LMT was measured (Figure 19a). We see in the false color plot that an island of optimum (i.e., yellow) laser performance occurs between MZI reflectivity of 0% and 100% with the LMT voltage set to approximately 0.6 V. As the LMT voltage increases, another hot spot occurs at MZI voltage of 3.5 V and LMT voltage of 4.5 V. We interpret the second hot spot occurring at another laser cavity mode. The 1D plot (Figure 19b) is a sampling of the laser performance at a LMT voltage set to approximately 2.2 V.

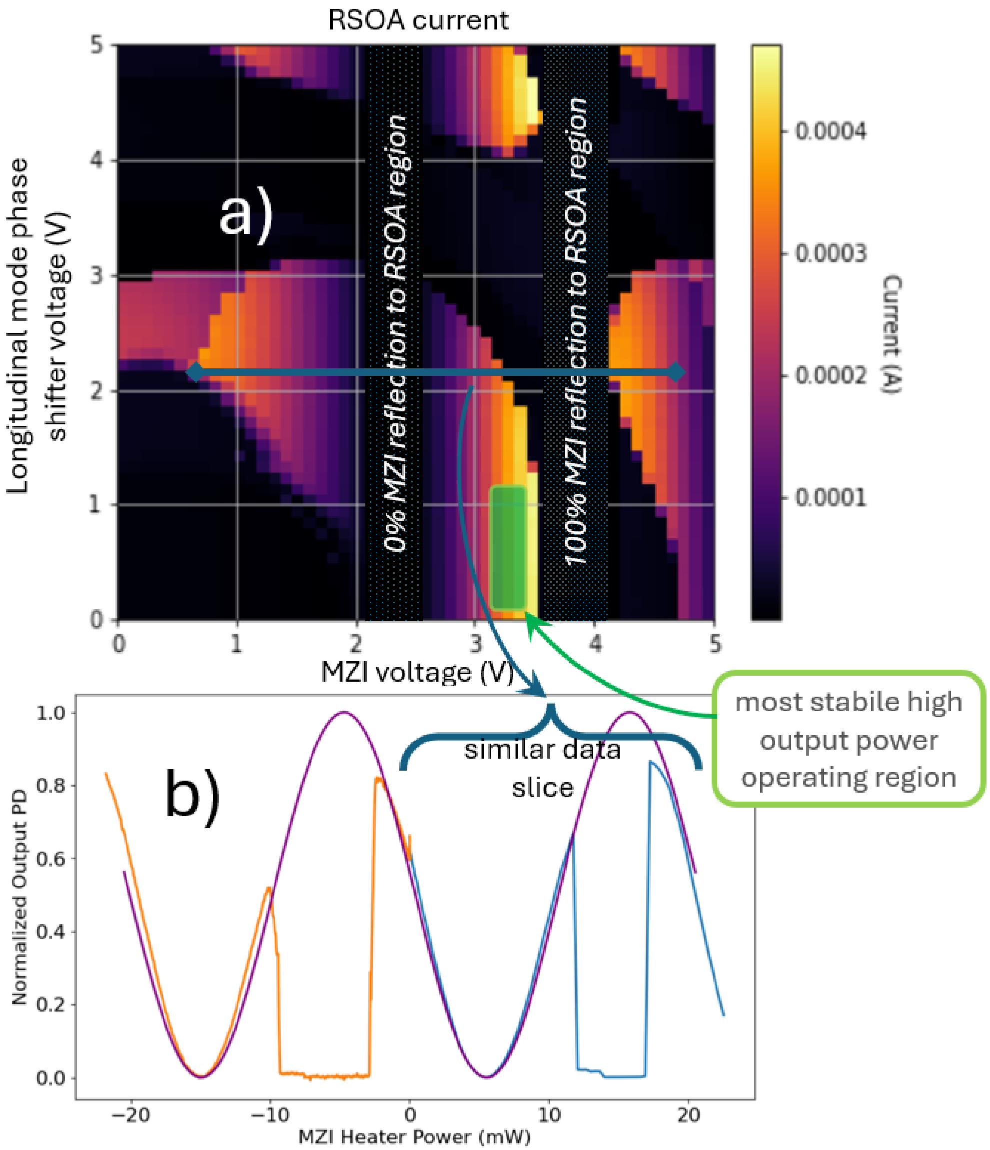

Figure 19. a) Plot of RSOA laser power with MZI (reflectivity) tuning and LMT voltage. b) RSOA laser power as a function of MZI power taken for LMT voltage set to zero.

9. Characterization of VR Performance

In preparation for the automatization of the RSOA ECL, a study was undertaken to determine the set of voltage combinations needed to power the 8- and 9-µm heater rings such that they would be resonant with each other. This process is called "ring mapping," which determined the wavelength voltage "coordinates" ($V_{8\mu m}$ and $V_{9\mu m}$) where lasing occurred.

We characterized the individual 8- and 9-µm ring wavelength responses by measuring the resonant wavelengths at a series of heater voltages (Figure 20). The next step was to run the ECL and record the ECL lasing wavelengths as the heater voltages of both rings were varied. As can be seen in Figure 21a, the laser peak powers (orange to purple) trace a series of tracks, similar to the paths of Figures 20a and 20b. The discontinuities along the curves of Figure 21a are due to regions of nonresonant cavity length. These discontinuities can be eliminated with use of the LMT.

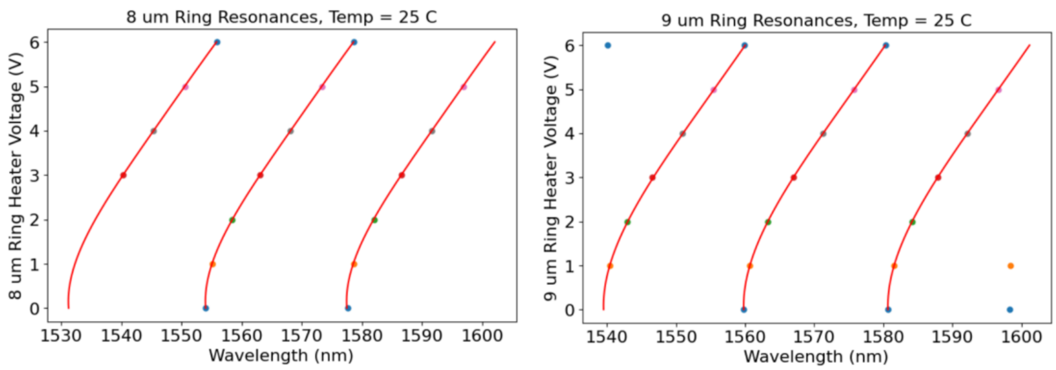

(a) (b)

Figure 20. Wavelength resonant response of the 8-µm ring and 9-µm VRs to heater voltage. The results of the two independent measurements are shown in Figure 16. The series of parallel curves are separated by the FSR of the rings.

To calculate the voltage coordinates at which the ECL could be expected to lase, the ring maps of Figures 21a and 21b were used to synthesize the data of Figure 20a, as shown in Figure 20b. Excellent agreement between experimental results (Figure 20a) and modeled prediction (Figure 20b) is evident.

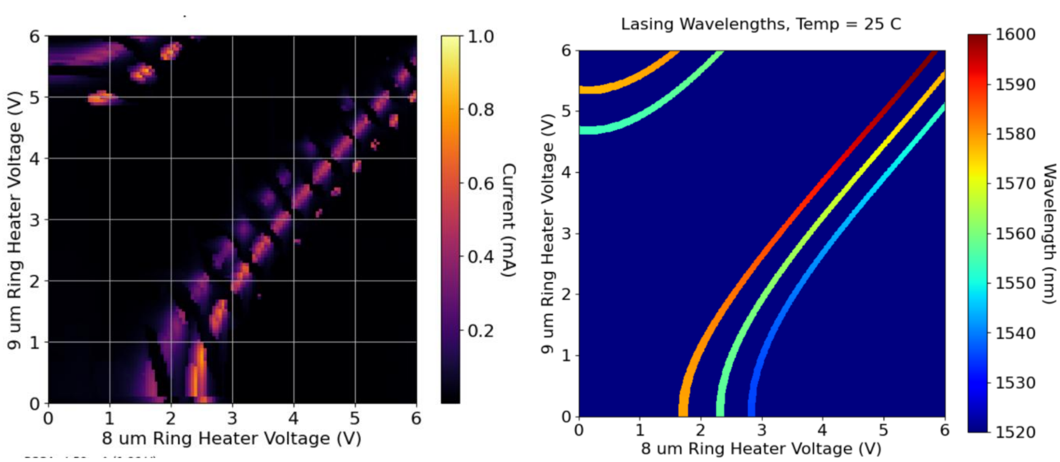

(a) (b)

Figure 21. a) Experimental comparison of the ECL power with swept ring voltage. b) Calculated map of VRs response as function of voltage with wavelength as a bar chart.

10. The 90/10 Splitter

The 90/10 DC shown in Figure 16 was characterized. At 1550 nm, the bar branch of the DC received 89% of the power and loss was negligible compared with our measurement resolution (Figure 22).

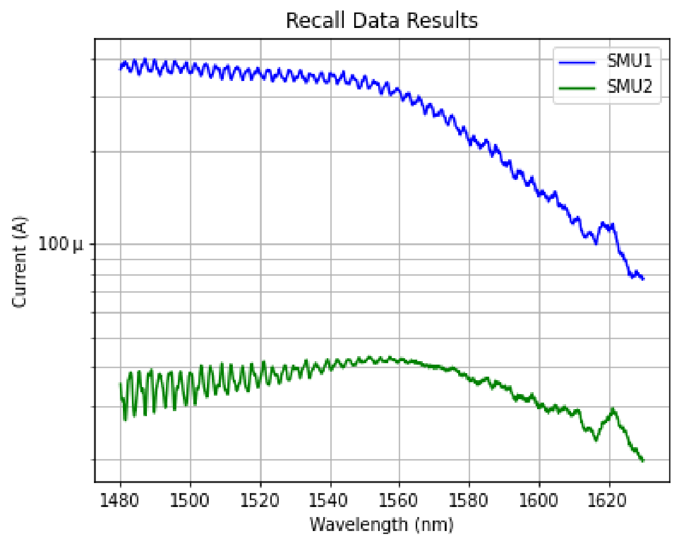

Figure 22. The wavelength dependent response of the 90/10 DC. The largest portion (89%) of the light leaving the ECL was directed towards the PD.

11. The PD Component

One Ge PD design was used for all detectors in the ECL. The responsivity (A/W) of the Ge detector decreased by 50% from 1500 to 1600 nm (Figure 23), as can be expected with the Ge PD. The evidence of regular ripples allowed us to estimate the back reflection of the PD using the following formula (Ghannam 2022):

$$R = \frac{\sqrt{ER} - 1}{\sqrt{ER} + 1} \quad (10)$$

where ER is the ratio of peak-to-trough intensity values. It was calculated that the back reflection $R \approx 1.5\%$ (18 dB). Biasing the PD in reverse showed onset of increased dark current after biasing the PD to 10 V. Therefore, it is recommended that the PD be reverse-biased to 9 V or below (Figure 23).

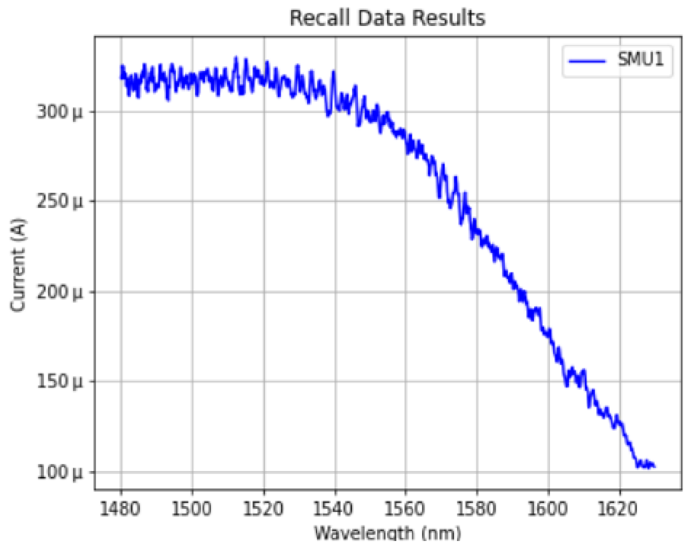

Figure 23. Measured photocurrent of the Ge PD as a function of wavelength.

12. Conclusion

We have characterized the performance of the ARL PIC ECL, tunable from 1530 to 1610 nm, with an EO efficiency of up to 6%, performance of 100 µW, and a SMSR of 60 dB. The components of the ECL have been detailed with their tuning characteristics and their performance modeled. We expect that with lower PWB chip-to-PIC loss, higher power with greater EO efficiency will be demonstrated.

13. References

Chu T, Fujioka N, Ishizaka M. Compact, lower-power-consumption wavelength tunable laser fabricated with silicon photonic wire waveguide micro-ring resonators. Opt Express. 2009;17(6):14063–14068.

Coldren LA, Verrinder PA, Klamkin J. A review of photonic systems-on-chip enabled by widely tunable lasers. IEEE J Quantum Electron. 2022;58:1–10.

Elshaari AW, Pernice W, Srinivasan K, Benson O, Zwiller V. Hybrid integrated quantum photonic circuits. Nat Photonics. 2020;14:285–298.

Ghannam I, Merget F, Witzens J. Silicon nitride C-band grating couplers with reduced waveguide back-reflection. Proc SPIE. 2022;12007. https://doi.org/10.1117/12.2607729

Milton A, Burns W. Mode coupling in optical waveguide horns. IEEE J Quantum Electron 1977;13:828–835.

Newman ZL et al. Architecture for the photonic integration of an optical atomic clock. Optica. 2019;5:680–685.

Roelkens G et al. Present and future of micro-transfer printing for heterogeneous photonic integrated circuits. APL Photonics. 2024;9:010901.

Smit M. Williams K, van der Tol J. Past, present, and future of InP-based photonic integration. APL Photonics. 2019;4:050901.

Strandberg E, Juodėnas M, Šípová-Jungová H, Käll M. Flat plasmonic biosensor with an on-chip metagrating-integrated laser. ACS Sens. 2025;10:7670–7678.

Xu D-X et al. Empirical model for the temperature dependence of silicon refractive index from O to C band based on waveguide measurements. Opt Express. 2019;27:27229–27241.

List of Symbols, Abbreviations, and Acronyms

1/3D	One-/Three-Dimensional
AIM	American Institute for Manufacturing Integrated Photonics
ARL	Army Research Laboratory
ASE	Amplified Spontaneous Emission
DC	Directional Coupler
DEVCOM	U.S. Army Combat Capabilities Development Command
EC	Edge Coupler
ECL	External Cavity Laser
EO	Electrical to Optical
FSR	Free Spectral Range
FWHM	Full Width at Half Maximum
Ge	Germanium
HOM	Higher Order Mode
IR	Infrared
LMT	Longitudinal Mode Tuner
MFD	Mode Field Diameter
MMI	Multi-Mode Intereferometer
MZI	Mach–Zehnder Interferometer
NA	Numerical Aperture
n_{eff}	Phase Velocity of Medium
Ø	Diameter
OPL	Optical Path Length
OSA	Optical Spectrum Analyzer
P	Power
PD	Photodiode
PIC	Photonic Integrated Circuit

PWB	Photonic Wire Bond
Q	Quality of resonator
R	Ring of Radius
RR	Ring Resonator
RSOA	Reflective Semiconductor Optical Amplifier
Si	Silicon
SiN	Silicon Nitride
SiO_2	Silicon Dioxide
SMSR	Side Mode Suppression Ratio
VR	Vernier Ring
ΔT	Change in Temperature
$\Delta\lambda$	Change in Wavelength
λ	Wavelength
λ_{FWHM}	FWHM Wavelength of Spectrum
φ	Phase

1 (PDF)	DEFENSE TECHNICAL INFORMATION CTR DTIC OCA
1 (PDF)	DEVCOM ARL FCDD RLB CB TECH LIB